BIOCHEMISTRY
including biophysical chemistry & molecular biology
Article

*Biochemistry* **2009,** *48,* 3915–3927 3915
DOI:10.1021/bi900075d

# Crystal Structure of the Acid-Induced Arginine Decarboxylase from *Escherichia coli*: Reversible Decamer Assembly Controls Enzyme Activity[†]

Juni Andréll,[‡] Matthew G. Hicks,[§,∥] Tracy Palmer,[§,⊥] Elisabeth P. Carpenter,[‡,#] So Iwata,*[,‡] and Megan J. Maher*[,‡,◇]

[‡]*Division of Molecular Biosciences, Imperial College, London SW7 2AZ, U.K., and* [§]*John Innes Centre, Norwich NR4 7UH, U.K.* [∥]*Present address: Department of Biological Sciences, University of East Anglia, U.K.* [⊥]*Present address: Division of Molecular and Environmental Biology, College of Life Sciences, University of Dundee, U.K.* [#]*Present address: MPL Group, Diamond Light Source, Didcot, U.K.* [◇]*Present address: Centenary Institute of Cancer Medicine and Cell Biology, Sydney, Australia.*

*Received January 18, 2009. Revised Manuscript Received March 18, 2009*

ABSTRACT: The acid-induced arginine decarboxylase is part of an enzymatic system in *Escherichia coli* that contributes to making this organism acid resistant. The arginine decarboxylase is a vitamin $B_6$-dependent enzyme that is active at acidic pH. It consumes a proton in the decarboxylation of arginine to agmatine, and by working in tandem with an arginine−agmatine antiporter, this enzymatic cycle protects the organism by preventing the accumulation of protons inside the cell. We have determined the structure of the acid-induced arginine decarboxylase by X-ray crystallography to 2.4 Å resolution. The arginine decarboxylase structure revealed a ca. 800 kDa decamer composed as a pentamer of five homodimers. Each homodimer has an abundance of acidic surface residues, which at neutral pH prevents inactive homodimers from associating into active decamers. Conversely, acidic conditions favor the assembly of active decamers. Therefore, the structure of arginine decarboxylase presents a mechanism by which its activity is modulated by external pH.

In order to infect a human host, enteric *Escherichia coli* must pass through the stomach, which has a pH of around 2.0, and survive there for approximately 2 h before the stomach is emptied. *E. coli* is capable of surviving in the highly acidic environment of the stomach since it possesses acid resistance (AR)[1] systems that protects cells in an environment of pH 2.5 and below (*1*). Three such acid resistance systems have been identified in *E. coli*: (1) oxidative glucose-repressed acid resistance (AR1), (2) glutamate-dependent acid resistance (AR2), and (3) arginine-dependent acid resistance (AR3) (*1*). The three AR systems work independently and are redundant, ensuring the survival of the stationary phase organism in a variety of acidic environments. The AR3 system has two components: the acid-induced biodegradative arginine decarboxylase (AdiA) and the arginine−agmatine antiporter (AdiC) (*2*, *3*). Both proteins are expressed at high levels in the cell at low pH in rich media (*4*). AdiA catalyzes the decarboxylation of one molecule of arginine into agmatine, consuming one proton in the process, and AdiC transports the agmatine out of the cell in exchange for arginine. Through this enzymatic cycle, AR3 acts to protect the organism by preventing the accumulation of protons inside the cell.

The decarboxylation reaction catalyzed by AdiA is dependent on the vitamin $B_6$ derived cofactor, pyridoxal 5′-phosphate (PLP). PLP is a common cofactor to enzymes primarily involved in the metabolism of amino acids. These PLP-dependent enzymes are capable of catalyzing a broad range of chemical reactions such as transamination, racemization, and elimination and replacement reactions in addition to decarboxylation. The PLP

[†]This work was supported by the European Union and the BBSCR. M.J.M. is a Cancer Institute of NSW Fellow. T.P. is an MRC senior non-clinical research fellow, and M.G.H. is an MRC-supported postdoc.

*Corresponding authors. S.I.: phone, +44 (0)2075943064; fax, +44 (0)2075941936; e-mail, s.iwata@imperial.ac.uk. M.J.M.: phone, +61 (0)295656280; fax, +61 295656101; e-mail, m.maher@centenary.org.au.

[1]Abbreviations: AdiA, acid-induced biodegradative arginine decarboxylase; AdiC, arginine−agmantine antiporter; AR, acid resistance; AspAT, aspartate aminotransferase; CadA, lysine decarboxylase; FPLC, fast protein liquid chromatography; GadB, glutamate decarboxylase; HEPES, 4-(2-hydroxyethyl)-1-piperazineethanesulfonic acid; MES, 2-(*N*-morpholino)ethanesulfonic acid; MIRAS, multiple isomorphous replacement with anomalous scattering; NCS, noncrystallographic symmetry; OrnDC, ornithine decarboxylase; PEG, polyethylene glycol; PLP, pyridoxal 5′-phosphate; SDS−PAGE, sodium dodecyl sulfate−polyacrylamide gel electrophoresis.


Published on Web 3/19/2009

cofactor is capable of slowly catalyzing many of these reactions in the absence of enzyme. The function of the protein is thus to provide substrate and reaction specificity and to enhance the catalytic properties of the PLP (*5*−*7*).

Similarly to AdiA, several other PLP-dependent decarboxylases are induced at low pH such as the biodegradative glutamate, histidine, ornithine, and lysine decarboxylases (*8*). These enzymes belong to fold type I of PLP enzymes (*7*, *9*). They can be further classified into different decarboxylase groups based on sequence analysis with the biodegradative glutamate and histidine decarboxylases belonging to group II and biodegradative basic amino acid decarboxylases arginine, ornithine, and lysine decarboxylases belonging to group III (*10*). The ornithine and lysine decarboxylases have been suggested to regulate cell pH through their consumption of protons in the decarboxylation reaction (*8*), similarly to arginine decarboxylase. However, only the acid resistance systems involving arginine decarboxylase (AdiA) (AR3) and glutamate decarboxylase (GadB) (AR2) confer acid resistance to *E. coli* when the external pH is as low as 2.5 (*1*). This has been suggested to be due to the lower pH optima of AdiA and GadB (5.2 and 4.6, respectively) compared with that of the *E. coli* lysine and ornithine decarboxylases (5.7 and 6.9, respectively) (*11*). This hypothesis is based on the observation that when the external pH is 2.5, the AR2 and AR3 systems elevate the internal pH of the bacterial cell from 3.6 to 4.2 and 4.7, respectively. These conditions correlate with the pH optima of 4.6 and 5.2 of GadB and AdiA, respectively.

Acid-inducible arginine decarboxylase (AdiA) has been characterized *in vitro* in two oligomeric states: as a dimer ($M_r$ 160000) and as a decamer ($M_r$ 820000) (*12*). The association of dimers into decamers is promoted by a number of solution conditions, including high concentrations of the enzyme itself, the presence of substrate analogues, divalent cations, high concentrations of monovalent cations, and acidic pH (pH $<6$) (*12*). Under conditions where the pH of the solution is greater than 6.5, and the concentration of monovalent cations is low (less than 0.04 M), the AdiA decamer dissociates into dimers (*12*). At the optimum pH for AdiA activity (pH 5.2), only the decameric form of the enzyme contributes to the reaction (*13*). Hence, the decameric form of AdiA dominates when *E. coli* is exposed to acidic conditions. In order to investigate the structural basis of this decameric assembly and its relationship to the regulation of AdiA activity, we have determined the crystal structure of AdiA from *E. coli* to 2.4 Å resolution. The AdiA structure shows an ~800 kDa decamer composed as a pentamer of five homodimers. The structure shows an abundance of acidic surface residues on the AdiA homodimer, which mimics charge distributions characterized for acidophilic proteins. We propose that under conditions of low pH the surface charge of individual, inactive homodimers is partially neutralized, allowing the assembly of AdiA into functional decamers. In this way, the structure of AdiA reveals the mechanism by which enzyme activity is regulated by cellular pH.

## EXPERIMENTAL PROCEDURES

*Purification of AdiA*. *E. coli* strain BL21(DE3) (*14*) was transformed with plasmid pREP4, which encodes the $lacI^q$ allele of the LacI repressor protein. This was transformed with plasmid pQE70 (Qiagen) containing the gene for an outer membrane protein. The cells were grown at 37 °C with shaking at 180 rpm in Luria−Bertani medium (1% tryptone, 0.5% yeast extract, 1% NaCl; supplied by Formedium of Norwich) supplemented with 0.2% glucose, ampicillin (100 μg/mL), and kanamycin (30 μg/mL) in unbuffered conical flasks. Typically, an overnight culture was used to inoculate 1 L of medium in a 2 L flask at a 1:100 dilution. Cultures were grown for 2−4 h to an $OD_{600}$ of ~0.4 when overexpression of the outer membrane protein was induced with 2 mM IPTG. Cells were grown for a further 3 h and then harvested at 5500 rpm in a Sorvall SLA6000 rotor. Cell pellets were combined and washed in 20 mM Na-HEPES, pH 8.0, and 150 mM NaCl (buffer 1). Cells were harvested again and pellets routinely frozen at −80 °C. Washed cell pellets were resuspended in buffer 1 at 3 mL/L of culture. Cell suspensions were disrupted by passage through a French pressure cell in the presence of Complete EDTA-free protease inhibitor (Roche), DNase, and lysozyme (Sigma). Cell debris was removed by centrifuging for 10 min at 7000 rpm in a Sorvall SS34 rotor. Cell envelopes were isolated by ultracentrifugation at 45000 rpm in a Beckman Ti70 rotor for 90 min. Protein concentration in crude cell envelopes resuspended in buffer 1 was determined using the Bio-Rad detergent-compatible assay kit, based on the method of Lowry (*15*). Crude cell envelopes were agitated for 1 h in the presence of 1% *N*-lauroylsarcosine in buffer 1, at 5−10 mg/mL of total cell envelope protein. AdiA was present mainly in a form resistant to *N*-lauroylsarcosine extraction. Insoluble material was removed by further ultracentrifugation at 45000 rpm in a Beckman Ti70 rotor for 60 min and then agitated for 1 h in 1% $C_8E_4$ detergent in buffer 1 at a protein concentration at 5−10 mg/mL of protein. Insoluble material was removed by a further 60 min ultracentrifugation step, as previously.

Soluble material was then applied to a 5 mL Hi-Trap chelating Ni column (GE Lifesciences) using an ÄKTA FPLC. For obscure reasons, AdiA bound to this nickel-chelating column. The column was washed in 12 mM imidazole (Fluka) in buffer 1 supplemented with 0.05% $C_8E_4$. A gradient of 12−150 mM imidazole in buffer 1 supplemented with 0.05% $C_8E_4$ over 6 column volumes was applied. AdiA eluted between 60 and 90 mM imidazole. Fractions containing AdiA were analyzed by SDS−PAGE using 10% polyacrylamide gels, with AdiA displaying a characteristic heat modifiability, converting to its monomeric mass of 87 kDa from a mass of $>250$ kDa after 5 min heat treatment in the loading buffer of Laemmli (*16*). Fractions containing AdiA were pooled and concentrated to a volume $<500$ μL and applied to a Superdex 200 HR10/30 gel-filtration column equilibrated in 20 mM Na-HEPES, pH 8.0, 50 mM NaCl, and 0.05% $C_8E_4$ and eluted at 0.5 mL/min. AdiA eluted at $>99\%$ purity between 8 and 11 mL. Samples containing AdiA were analyzed by SDS−PAGE.

Table 1: Data Collection and Refinement Statistics

| | data set | | |
|---|---|---|---|
| | native AdiA | Pb-AdiA | Hg-AdiA |
| *Data Collection and Processing* | | | |
| space group | $P6_4$ | $P6_4$ | $P6_4$ |
| cell dimensions *a*, *c* (Å) | 197.7, 450.3 | 198.3, 449.8 | 197.7, 449.9 |
| soaking concn and time | | 2 mM, 45 h | 1 mM, 45 h |
| ESRF beamline | ID14-4 | ID14-3 | ID14-1 |
| wavelength (Å) | 0.93 | 0.93 | 0.93 |
| resolution range (Å) | 50.0−2.4 | 50.0−3.0 | 50.0−3.5 |
| measured reflections | 1913962 | 1147010 | 904555 |
| unique reflections | 385411 | 388656 | 117365 |
| completeness (%)[a] | 99.9 (100.0) | 98.6 (97.4) | 93.4 (87.2) |
| redundancy | 5.0 | 3.0 | 7.7 |
| $I/\sigma(I)$[a] | 10.7 (2.3) | 9.8 (2.2) | 14.3 (3.1) |
| $R_{sym}$[b] (%)[a] | 15.0 (78.5) | 10.4 (38.5) | 15.7 (58.3) |
| *Model Refinement* | | | |
| resolution (Å) | 2.4 | | |
| $R_{work}$[c] (%)[a] | 17.7 (25.4) | | |
| $R_{free}$[d] (%)[a] | 22.9 (31.8) | | |
| average *B* factor (Å$^2$) | 23.6 | | |
| phasing power[e] ISO (acentric/centric) | | 1.21/0.95 | 0.78/0.70 |
| phasing power[e] ANO | | 0.24 | 0.37 |
| *Stereochemistry* | | | |
| rmsd for bond length (Å) | 0.014 | | |
| rmsd for bond angles (deg) | 1.464 | | |
| *Residues in Ramachandran plot*[f] | | | |
| favored regions (%) | 97.3 | | |
| allowed regions (%) | 100.0 | | |

[a] Statistics for the highest resolution shell are given in parentheses. [b] $R_{sym} = \sum_h \sum_i |I_{hi} - \langle I_h \rangle| / \sum_h \sum_i |I_{hi}|$. [c] $R_{work} = \sum |F_o - F_c| / \sum F_o$ for all reflections. [d] $R_{free} = \sum |F_o - F_c| / \sum F_o$ calculated using randomly selected reflections (5%). [e] Phasing power: $|F_{H(calc)}|$/phase-integrated lack of closure. The overall figure of merit is (acentric/centric) = 0.25/0.28. [f] Ramachandran plot values as assessed by MOLPROBITY.

*Crystallization*. Crystallization conditions were screened at 293 K, according to the sparse matrix method (*17*), using commercially available screens (MemStart/MemSys from Molecular Dimensions) and the sitting drop vapor diffusion technique. Screens were set up in 96-well plates (MRC 2-well plates from SwisscI) using a Cartesian Microsys robot. Drops consisted of protein (0.2 $\mu$L) with an equal volume of reservoir solution. Initially, crystals were observed in condition 43 of the MemStart screen (100 mM MES, pH 6.5, 10% PEG 8000, and 200 mM sodium acetate). Further refinement of the crystallization conditions produced crystals of typical dimensions 0.1 × 0.2 × 0.4 mm$^3$, which were grown by mixing the protein solution (0.2 $\mu$L, 13 mg/mL in 20 mM HEPES, pH 8.0, 50 mM sodium chloride, and 0.05% $C_8E_4$ detergent) with an equal volume of reservoir solution (100 mM MES, pH 6.5, 13% PEG 8000, and 400 mM sodium acetate). Typically, crystals grew to their maximum dimensions in 3−5 days.

Crystals of AdiA were cryoprotected by transferring each crystal into drop solution (1 $\mu$L, 100 mM MES, pH 6.5, 13% PEG 8000, 400 mM sodium acetate, 20 mM HEPES, pH 8.0, 50 mM sodium chloride, and 0.05% $C_8E_4$) and increasing the glycerol content of the drop to a final concentration of 20% in ca. 7% increments. The crystal was briefly immersed into a second drop (1 $\mu$L) containing 20% glycerol, immediately prior to transfer into liquid nitrogen.

Lead- and mercury-derivatized crystals of AdiA were prepared by transferring individual crystals into drop solution (2−3 $\mu$L, 100 mM MES, pH 6.5, 13% PEG 8000, 400 mM sodium acetate, 20 mM HEPES, pH 8.0, 50 mM sodium chloride, and 0.05% $C_8E_4$ detergent) containing trimethyllead acetate ($PbMe_3$) (2 mM final concentration) or mercuric chloride ($HgCl_2$) (1 mM final concentration), respectively. The crystals were soaked for a total of 45 h and were cryoprotected as described including $PbMe_3$ or $HgCl_2$ in the cryo buffer.

*Data Collection*. X-ray data were collected from frozen crystals at 100 K at the ESRF. Diffraction data were collected from a crystal of native AdiA (native AdiA, Table 1) on beamline ID14-4 on a Q315r ADSC CCD image-plate detector at a fixed wavelength of 0.93 Å. A data set from a crystal soaked in $HgCl_2$ (Hg-AdiA, Table 1) was collected on beamline ID14-1 on an ADSC Q210 CCD image-plate detector at a fixed wavelength of 0.93 Å. A data set from a lead-soaked crystal (Pb-AdiA, Table 1) was collected on beamline ID14-3 on a Q4R ADSC CCD image-plate detector at a fixed wavelength of 0.93 Å. The data was processed using the HKL suite of programs, DENZO and SCALEPACK (*18*). Data collection statistics are presented in Table 1.

*Structure Determination*. The 2.4 Å resolution structure of AdiA was solved by MIRAS methods using data from crystals soaked in solutions containing $PbMe_3$ or $HgCl_2$. The positions of 10 Pb atoms in the Pb-AdiA data were

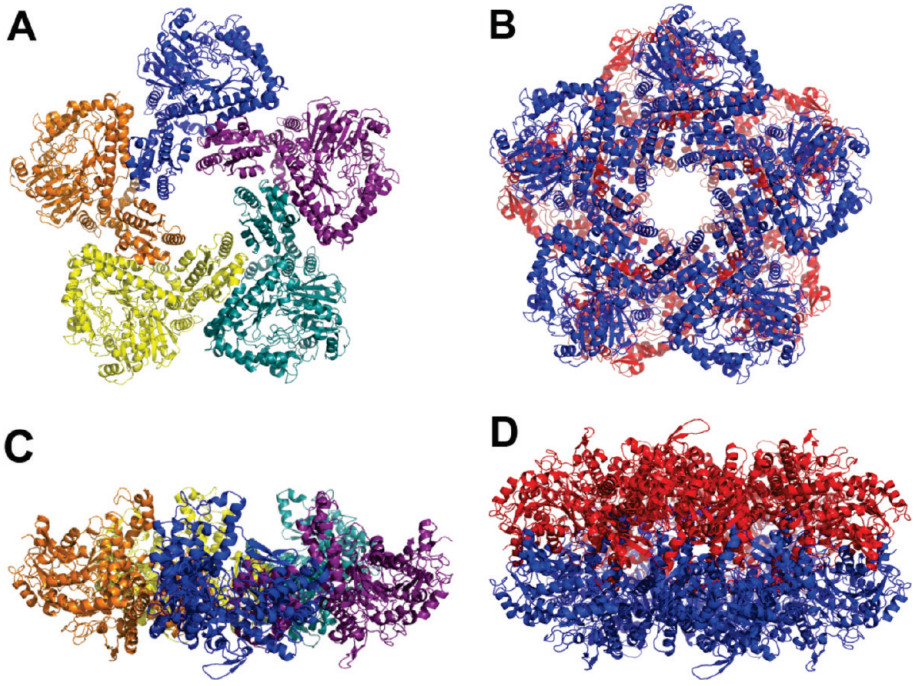


FIGURE 1: AdiA decamer. (A) AdiA pentameric ring, chains A−E, bottom view. One pentameric ring is half the content of the asymmetric unit. Molecule A (blue), molecule B (violet), molecule C (red), molecule D (yellow), molecule E (orange). (B) AdiA decamer, bottom view. (C) AdiA pentameric ring, chains A−E, side view. (D) AdiA decamer, side view. Chains A−E (blue), chains A*−E* (red).

determined by direct methods, with SHELXD (*19*), using isomorphous differences between the Pb-AdiA and native AdiA data. These sites were used to calculate initial SIRAS phases to the resolution limit of the data (3.0 Å) using the program SHARP (*20*). A 5-fold NCS averaging matrix was calculated by RESOLVE (*21*) using the coordinates of the Pb heavy atom positions. Density modification carried out to 3.0 Å resolution using the program DM with solvent flattening histogram mapping and averaging options (*22*) was used to improve the initial Pb-SIRAS phases. This yielded an interpretable electron density map.

In order to improve the quality of the experimental electron density map further, an additional 20 Hg atom positions were identified in anomalous difference Fourier maps calculated with the Hg-AdiA data and the SIRAS phases from the Pb derivative. SHARP was used to calculate MIRAS phases using a total of 10 Pb and 20 Hg sites. The refined Pb coordinates were used to calculate a 10-fold NCS averaging matrix, and density modification was carried out using the program DM, with phase extension to 2.4 Å, the resolution of the native AdiA data.

*Model Building*. An incomplete initial model of AdiA was built using automatic modeling programs BUCCANEER (*23*) and ARP-wARP (*24*). Further model building, to complete the trace of AdiA chain A, was carried out in COOT (*25*), using the structure of the paralogue ornithine decarboxylase (PDB entry 1ORD) (*26*), modified with CHAINSAW (*27*), as a template. Applying individual components of the 10-fold NCS matrix using PDBSET generated AdiA chains B−K. Initial rigid body and restrained refinement in REFMAC5 (*28*) gave residuals for the initial model of $R_{work}$ = 40% and $R_{free}$ = 37%. Tight NCS restraints were applied throughout subsequent rounds of refinement in REFMAC5. The model was improved upon by iterative cycles of model building and map calculation. The NCS restraints were removed, and TLS refinement (*29*) was applied for each chain in the last cycles of refinement. Data to 2.4 Å resolution were included for the native data set in spite of a high $R_{sym}$ in the highest resolution shell (78.5%) since the refined structure shows reasonable residuals of $R$ = 27.2% and $R_{free}$ = 33.5% in the highest resolution shell (Table 1). The coordinates and structure factors were deposited with the Protein Data Bank as PDB entry 2VYC.

The coordinates of the agmatine aldimine in Figure 6A were taken from the structure of the arginine decarboxylase from *Paramecium bursaria* Chlorella virus, PDB entry 2NV9 (*30*). The arginine agmatine was modeled into the AdiA active site by matching the pyridine ring of the agmatine aldimine with the pyridine ring of the AdiA PLP cofactor in COOT.

## RESULTS

*Quality of the AdiA Model*. The structure of AdiA was solved by the MIRAS method using data from a native crystal and crystals derivatized with lead and mercury. The structure was refined to 2.4 Å resolution. Refinement of the model converged with residuals $R$ = 17.7% and $R_{free}$ = 22.9%. The model shows good geometry with 97.3% of residues in the most favored region of the Ramachandran plot as assessed by MOLPROBITY (*31*) (Table 1). The asymmetric unit contains 10 molecules, chains A−J. They are organized as two pentameric ring structures, chains A−E and F−J (Figure 1A,C). The 10 identical molecules, chains A−J, in the asymmetric unit superpose with an average rmsd value of 0.2 Å for 755 common Cα atoms, which is consistent with the

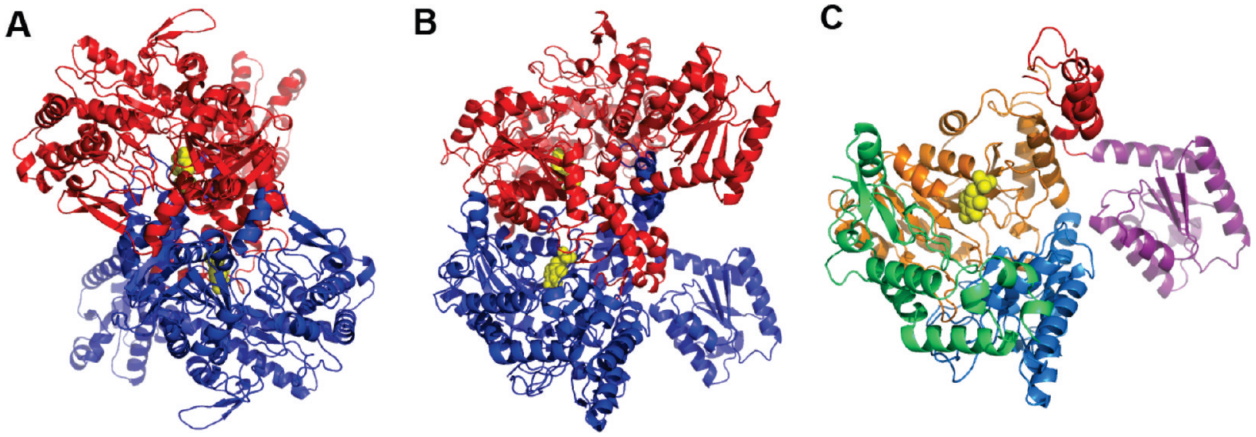


FIGURE 2: AdiA homodimer. (A) AdiA (AC*) dimer, front view. Molecule A (blue), molecule C* (red), PLP cofactor (yellow spheres). (B) AdiA (AC*) dimer, side view. (C) AdiA monomer (molecule A) in same orientation as in (B). Wing domain, residues 1−139 (purple); linker domain, residues 140−192 (red); PLP-binding domain, residues 193−439 (orange), AspAT-like small domain, residues 400−608 (blue); carboxy-terminal domain, residues 609−755 (green).

resolution of the structure and the fact that noncrystallographic symmetry restraints were applied until the last cycles of refinement. Altogether, the asymmetric unit contains 7550 protein residues, 2568 water molecules, and 10 pyridoxal 5′-phosphate (PLP) molecules. For the bulk of the structure, the electron density is very well defined, which allowed all 755 protein residues per chain to be modeled. The average temperature factor of the model (all atoms) is $B = 23.6$ Å$^2$.

*The AdiA Decamer and Dimer*. AdiA crystallizes with two pentameric rings in the asymmetric unit in space group $P6_4$ (Figure 1A,C). The application of the $P6_4$ symmetry operators creates six decamers per unit cell, where the two pentameric rings of each decamer are related by a crystallographic 2-fold axis (Figure 1B,D). The basic unit of AdiA, similar to other PLP enzymes, is a dimer. The AdiA decamer is assembled from five homodimers arranged with 5-fold noncrystallographic symmetry into a pentamer of dimers. It has a diameter of ~180 Å, is ~100 Å high, and contains a central hole of ~30 Å diameter. The structure of an AdiA dimer in isolation (here molecule A and symmetry-related molecule C*) shows a compact globular "core" structure, with protruding wing domains from each monomer (Figure 2A,B). The AC* dimer has dimensions of approximately 100 × 55 × 55 Å.

*The AdiA Monomer*. The structure of AdiA is homologous to the structure of the biodegradative ornithine decarboxylase (OrnDC) from *Lactobacillus* 30a (*26*), and the two enzymes share 31% sequence identity. For clarity, the same terminology used by Momany et al. to describe OrnDC will be employed when appropriate when discussing the structural organization of AdiA. Since the 10 AdiA molecules in the asymmetric unit are identical, within experimental error, only molecule A will be discussed here.

Molecule A consists of one polypeptide chain, residues 1−755, which can be divided into five domains: (1) the amino-terminal wing domain (residues 1−139), (2) the linker domain (residues 140−192), (3) the PLP-binding domain (residues 193−439), (4) the aspartate aminotransferase- (AspAT-) like small domain (residues 440−608), and (5) the carboxy-terminal domain (residues 609−755) (Figure 2C). The PLP-binding domain, the AspAT-like small domain, and the carboxy-terminal domain form an open bowl-like structure, where each domain roughly forms a third of the "bowl". The wing domain extends from the "bowl" like a handle, while the linker domain protrudes away at approximately 90° relative to the other domains (Figure 2C).

The wing domain, residues 1−139, has a central parallel $\beta$-sheet consisting of five $\beta$-strands flanked by six α-helices: two on each face of the sheet (α1α6 and α2α3) and two at the C-terminal edge of the sheet (α4α5). The linker domain, residues 140−192, is a small domain that consists of three α-helices (α7, α9, α10) and a $3_{10}$-helix (α8) connected by loops and turns. The PLP-binding domain, residues 193−439, is the largest domain and consists of a seven-stranded mixed $\beta$-sheet ($\beta$6−$\beta$12) and seven α-helices (α11−α17) in a conserved type I PLP enzyme fold. The PLP cofactor is bound at the C-terminal end of the $\beta$-sheet in a manner similar to other type I PLP enzymes. The fold of the AspAT-like small domain, residues 440−608, is similar to that of the small domain of AspAT (PDB entry 1C9C; Ishijima, 2000) in that the cores of the structures superpose with each other with an rmsd of 2.6 Å for 82 aligned Cα atoms. However, the extensive loop regions (loop α19−$\beta$15, residues 506−535; loop $\beta$15−α20, residues 540−556), the small two-stranded $\beta$-sheet, and the small helix α19 present in this domain in AdiA do not exist in the small domain of AspAT. Finally, the carboxy-terminal domain, residues 609−755, consists of five α-helices (α22−α27) and a curved three-stranded antiparallel $\beta$-sheet ($\beta$18−$\beta$20). A domain equivalent to the AdiA carboxy-terminal domain is found in the homologous structure of OrnDC from *Lactobacillus* 30a (PDB entry 1ORD) (*26*) but not in the AspATs nor in any other protein in the Protein Data Bank according to a SSM search (*32*). Hence this domain appears unique to the group of basic amino acid decarboxylases to which AdiA and OrnDC belong. The five domains associate with each other through hydrogen bonds and electrostatic interactions.

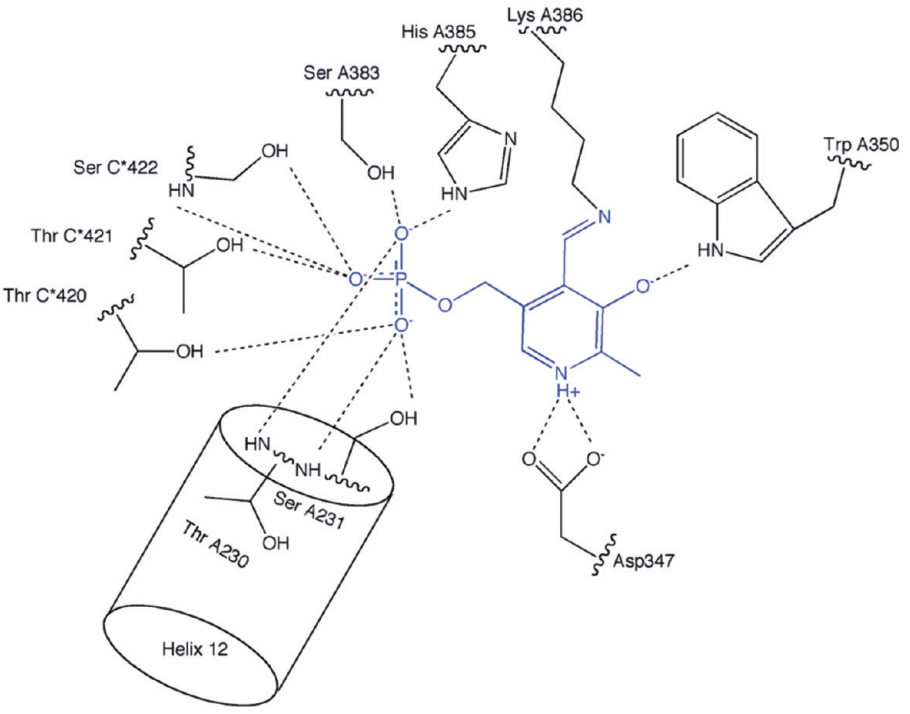


FIGURE 3: PLP coordination in the AdiA active site. The phosphate group of the PLP cofactor is coordinated by nine hydrogen bonds. Atom OP1 is coordinated by three hydrogen bonds to the side chains of residues His A385, Ser A383, and the main chain amide of residue Thr A230. Atom OP2 is coordinated by three hydrogen bonds to the side chain of Thr C*421 and the side chain and main chain amide of Ser C*422. Atom OP3 is coordinated by three hydrogen bonds to the side chain of Thr C*420 and the side chain and main chain nitrogen of Ser A231. The N atom of the pyridine ring forms a salt bridge with Asp A347, and the indole of Trp A350 forms a hydrogen bond to the pyridine ring 3-oxygen. The figure was generated by the program ChemDraw.

*The Active Site*. The formation of the AC* dimer effectively buries the active sites of each molecule ~30 Å from the dimer surface. There are two active sites per dimer that are located at the dimer interface ~20 Å apart. The PLP cofactor is partially solvent accessible through a deep cleft formed between the carboxy-terminal domain of molecule A and the PLP-binding domain of molecule C* in the AC* dimer. The PLP cofactor is covalently bound to the conserved residue Lys A386 forming a Schiff's base. Residues from both molecules A and C* coordinate the PLP phosphate group with nine hydrogen bonds in total (Figure 3). The PLP pyridine ring is sandwiched between the imidazole side chain of residue His A255 and the methyl group side chain of Ala A349. The N atom of the pyridine ring forms an electrostatic interaction with Asp A347, and the indole of Trp A350 forms a hydrogen bond to the pyridine ring 3-hydroxyl group. The PLP cofactor is thus tightly bound and oriented in the AC* dimer via a covalent bond, tight coordination of the phosphate group, and several interactions with the pyridine ring.

*Stabilization of the Decameric Structure*. The decameric structure as a pentamer of dimers is stabilized by the tight packing within dimers and by interactions made between the wing domains of neighboring molecules in each pentameric ring. The buried surface area between the two molecules in the AC* dimer is extensive at 5233 $Å^2$ per molecule, which corresponds to 16.4% of the solvent-accessible area of the molecule. Molecules A and C* form an extensive network of interactions with each other, consistent with their tight packing as a dimer. In the decamer, the dimers pack against each other via the wing domains. For example, in pentamer A−E, molecule A is flanked by molecule B and molecule E. The molecule A wing domain forms close interactions with both molecules B and E (Figure 1A). The molecule A wing domain packs against the AspAT-like small domain of molecule E, forming two salt bridges and five hydrogen bonds. It also packs against the wing domains of both molecules B and E via one salt bridge and a hydrogen bond to each neighboring wing domain. Altogether, the molecule A wing domain forms four salt bridges and seven hydrogen bonds to molecules B and E. Equivalent contacts are made between the wing domains of each molecule to neighboring molecules in the pentameric ring. The extensive interactions within dimers and between dimers stabilize the AdiA decameric structure. Overall, 24.9% (7965 $Å^2$) of the surface area of molecule A is buried within the decamer through the extensive interactions with the flanking molecules B and E and with the symmetry-related molecule C*.

## DISCUSSION

The PLP enzymes referred to in this discussion are summarized in Table 2.

*AdiA Decamer Assembly Regulates Enzyme Activity*. The AdiA structure determined at 2.4 Å resolution shows that AdiA assembles as an ~800 kDa decamer composed as a pentamer of dimers. This structural organization corresponds well with the model proposed by Boeker et al. and with what has previously been observed in electron micrographs (*12*, *33*). It is also consistent with analytical ultracentrifugation results and kinetic studies of dimer dissociation (*12*, *13*, *33*, *34*). These kinetic studies have

Table 2: Fold Type I PLP Enzymes

| enzyme | | organism | classification | PDB entry | ref |
|---|---|---|---|---|---|
| aspartate aminotransferase | AspAT | chicken | aminotransferase enzyme | 2AAT | *54* |
| dialkylglycine decarboxylase | DGD | *B. cepacia* | aminotransferase enzyme | 2DKB | *55* |
| DOPA decarboxylase | DDC | pig | group II decarboxylase | 1JS3, 1JS6 | *56* |
| glutamate decarboxylase | Gad67 | human | group II decarboxylase | 2OKJ | *57* |
| glutamate decarboxylase | GadB | *E. coli* | group II decarboxylase | 1PMM, 1PMO | *51* |
| ornithine decarboxylase | OrnDC | *Lactobacillus* 30a | group III decarboxylase | 1ORD, 1C4K | *26*, *47* |
| arginine decarboxylase | AdiA | *E. coli* | group III decarboxylase | 2VYC | this study |

shown that the assembly of the AdiA decamer is required for enzyme activity under acidic conditions. That is, when the pH of the cell decreases below pH ~6.0, the enzyme associates from inactive dimers into functional decamers. These decamers dissociate into inactive dimers at pH 6.5 or above (*12*, *13*). Decamer association is also favored by an increase in the concentration of the enzyme itself and by increases in substrate concentration and/or ionic strength, such as an increase in the concentration of sodium ions (*12*, *13*). The dissociation of the AdiA decamer into inactive dimers at neutral pH is likely to serve as a regulatory mechanism to ensure that AdiA is only active in the cell as the internal pH becomes more acidic (*34*).

In the present work, AdiA was crystallized at pH 6.5 from solutions with high protein (~13 mg/mL) and sodium ion concentrations (400 mM). These conditions favor the decameric form of the enzyme, which is consistent with the observation of AdiA decamers in the crystals. In principle, conditions of increased ionic strength generally promote protein subunit dissociation, rather than association (*35*). The fact that an increase in ionic strength promotes the association of AdiA from dimers into decamers suggests that charge repulsion needs to be overcome for assembly to take place (*36*). Indeed, the AdiA homodimer (for example, AC*) shows a net negative charge of −80, which results from the presence of 184 solvent-accessible acidic residues compared with 104 solvent-accessible basic residues (Figure 5). The calculated p*I* for the AdiA homodimer is 4.44 (*33*), which reflects this excess of acidic residues.

Interestingly, 25% of the solvent-accessible acidic residues of each homodimer are located in their wing domains (23 solvent-accessible acidic residues (11 Glu plus 12 Asp) versus 11 solvent-accessible basic residues (7 Arg plus 4 Lys) per wing domain). Hence, the wing domains carry a strong negative electrostatic potential at neutral pH. We have shown through the crystal structure of AdiA that decamer formation is mediated exclusively by interactions between wing domains of neighboring homodimers. It follows that acidic conditions favor decamer assembly through neutralization of acidic surface residues in the wing domains. The acid resistance activity of AdiA is therefore double-edged. The protein itself acts as a biological buffer in its uptake of protons, leading to the assembly of active AdiA decamers, in addition to consuming protons in the decarboxylation reaction. Closer to neutral pH, the negative charges of the acidic residues would promote decamer disassembly by repelling each other. In particular, the packing interface between the wing domain and the AspAT-like domain in the decamer would be disrupted by the close proximity (5−7 Å) of the negative charges of the carboxylate groups of residues Asp102, Asp104 (molecule A), and Glu467 (molecule E).

The AR3 system in *E. coli* mimics strategies commonly used by acidophilic organisms to cope with acidic growth conditions. For example, the AR3 system is known to cause reversal of the membrane potential from negative to positive, which is a strategy observed in acidophiles proposed to deter the entry of protons into the cell (*11*). In addition, the abundance of acidic surface residues in AdiA is a common feature of many acidophilic proteins (*37*−*40*).

*The AdiA Active Site and Substrate Specificity*. The active site coordination of the PLP cofactor in AdiA shows features conserved among fold type I PLP-dependent enzymes. For instance, (1) the PLP phosphate group is bound to the N-terminus of an α-helix (AdiA-α12), where the helix dipole stabilizes the negative charge of the phosphate group, (2) a lysine residue (AdiA-Lys386) forms a covalent Schiff base linkage with the C4′ atom of the pyridine ring, (3) an aromatic residue (AdiA-Trp350) and an alanine residue (AdiA-Ala349) are involved in binding the pyridine ring, and (4) an apartate residue (AdiA-Asp347) forms a salt bridge with the protonated nitrogen of the pyridine ring (Figure 3).

The AdiA decarboxylation reaction most likely proceeds according to the generally accepted reaction coordinate of PLP enzymes (Figure 4) (*5*, *7*). The proton consumed in the AdiA decarboxylation reaction is donated by an as yet unidentified residue in the active site. It has been shown in kinetic experiments for fern L-methionine decarboxylase that a monoprotic acid protonates Cα in the decarboxylation reaction (*41*). For AdiA, it was suggested that a histidine residue, which can act as a monoprotic acid, would be the most likely candidate for protonating Cα (*42*). The histidine next in sequence to the internal aldimine forming lysine (AdiA-His385) is an unlikely candidate for the proton-donating residue, since it is involved in coordinating the phosphate. A more likely candidate, upon examining the AdiA active site, is the residue His255. His255 would be ideally positioned as a proton donor as it is the active site histidine residue located closest to the C4′ position of the pyridine ring with its side chain imidazole amide within a distance of 4 Å. The His255 residue is conserved among PLP-dependent decarboxylases (*43*) and is found in this position in all the fold type I PLP-dependent decarboxylase structures determined to date (Table 2), with the exception of the inducible glutamate decarboxylase (GadB) from *E. coli* that has a glutamine residue in

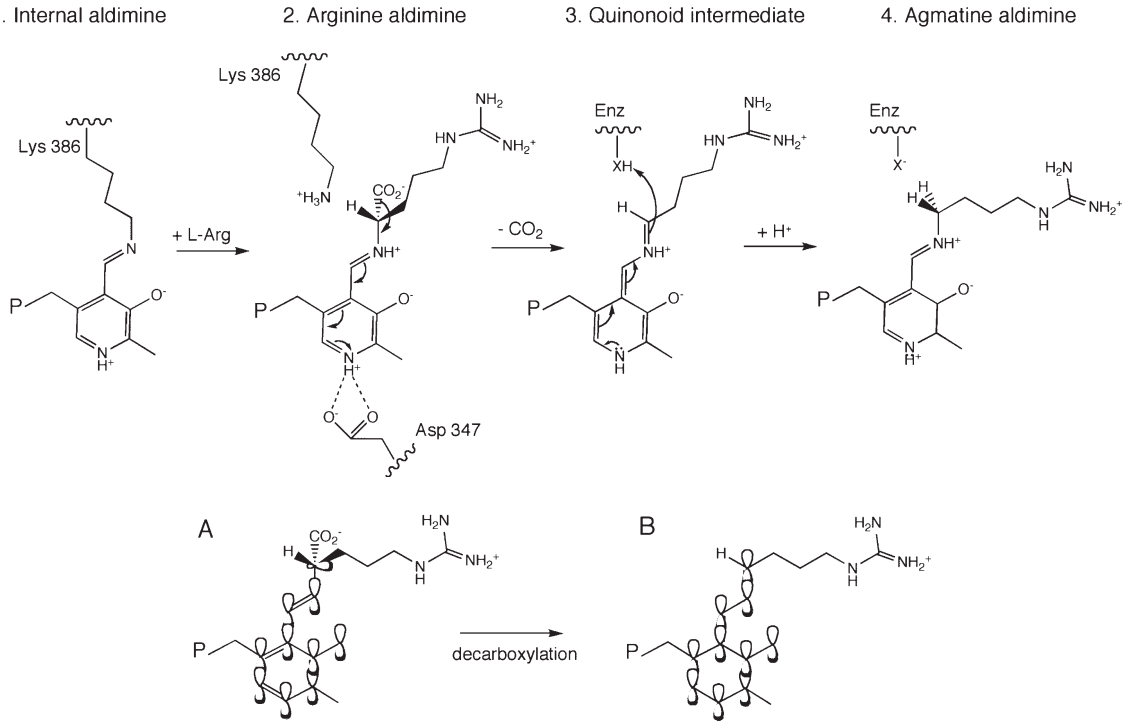


FIGURE 4: AdiA reaction coordinate. (1) In the resting state of the enzyme Lys386 forms an internal aldimine with the PLP cofactor. The Lys386 residue will be displaced in a transimination reaction by the substrate L-arginine, forming an arginine aldimine (2) with the PLP cofactor through a covalent bond between the C4′ position of the pyridine ring and the amino group of L-arginine. The L-arginine Cα−$COO^-$ bond to be broken in the decarboxylation reaction is predicted to align perpendicularly to the PLP pyridine ring (A), based on the Dunathan stereoelectric hypothesis and structural studies of substrate-bound dialkylglycine decarboxylase (*58*). This orientation allows for maximum overlap between the $\sigma$ orbitals of the bond to be broken and the $\pi$-system of the PLP pyridine ring. This minimizes the energy of transition state for bond breaking, which makes the Cα−$COO^-$ bond the most likely Cα bond to be broken. As the Cα−$COO^-$ bond is broken, the developing charge at the Cα position, caused by the loss of $CO_2$, is stabilized by delocalization within the extended conjugated $\pi$-system of the pyridine ring. The pyridine nitrogen acts as an electron-withdrawing group facilitating the breakage of the Cα−$COO^-$ bond. The Asp347 residue provides a stabilizing negative charge to the protonated pyridine nitrogen, which enhances the electron-withdrawing properties of the cofactor. The Cα−$COO^-$ bond breakage produces the quinonoid intermediate (3), in which the conjugated $\pi$-system is extended from the pyridine ring to the Cα of the substrate aldimine (B). The quinonoid intermediate is protonated at Cα by an unidentified residue in the active site to form the agmatine aldimine (4). The product agmatine is released from the enzyme as the internal aldimine between Lys386 and the PLP cofactor is re-formed. The figure was generated with the program ChemDraw.

this position. The absence of a histidine in this position in GadB, together with a catalytically active DOPA decarboxylase mutant, where the histidine residue in this position was mutated to a glutamine (*44*), suggests a different role for His255 than as the proton-donating residue. Hence, the identity of the proton-donating residue in AdiA remains to be confirmed.

Within the dimer, AdiA has an open active site where the PLP cofactor is clearly visible through a cleft formed between the carboxy-terminal domain of one monomer and the PLP-binding domain of the other (Figure 5). The ridge of the cleft formed by the carboxy-terminal domain is lined with negatively charged residues Glu735, Glu737, and Glu739 along the α26−$\beta$19 loop that runs from the surface of the molecule toward the interior of the active site. These negatively charged glutamate residues could serve to attract the positively charged substrate L-arginine into the active site.

In AspAT from *E. coli*, the main determinants for enzyme substrate specificity are two arginine residues that coordinate the side chain carboxylate groups of the substrates glutamate and aspartate (*45*). It is reasonable to expect that, in AdiA, negatively charged glutamate and/or aspartate residues would coordinate the positively charged guanidinium group of the L-arginine substrate. Accordingly, a substrate (agmatine aldimine) molecule can comfortably be modeled into the active site of AdiA (Figure 6). This approximate model puts the side chain guanidinium group of the agmatine aldimine approximately 5−6 Å from the side chain carboxylate groups of residues Glu A739 and Asp C*202. These are the closest glutamate and/or aspartate residues in the active site to the C4′ atom of the pyridine ring. PLP-dependent enzymes generally form a closed conformation around the bound substrate (*5*). In AdiA, closing the cleft around the active site is likely to bring residues Glu A739 and Asp C*202 within coordinating distance of the guanidinium group of arginine or agmatine aldimine. This would be analogous to the situation in AspAT where the closed conformation brings the substrate-coordinating residue Arg386 closer to the coenzyme.

The observations suggest that the carboxy-terminal domain would contribute to AdiA substrate specificity in two ways: (1) it would attract the doubly charged L-arginine species to the active site through glutamate residues lining the active site cleft, and (2) one of these residues (Glu739) would coordinate the guanidinium group of the arginine or agmatine aldimine reaction intermediates in the substrate-bound, closed conformation of the enzyme. It follows that the maximal activity

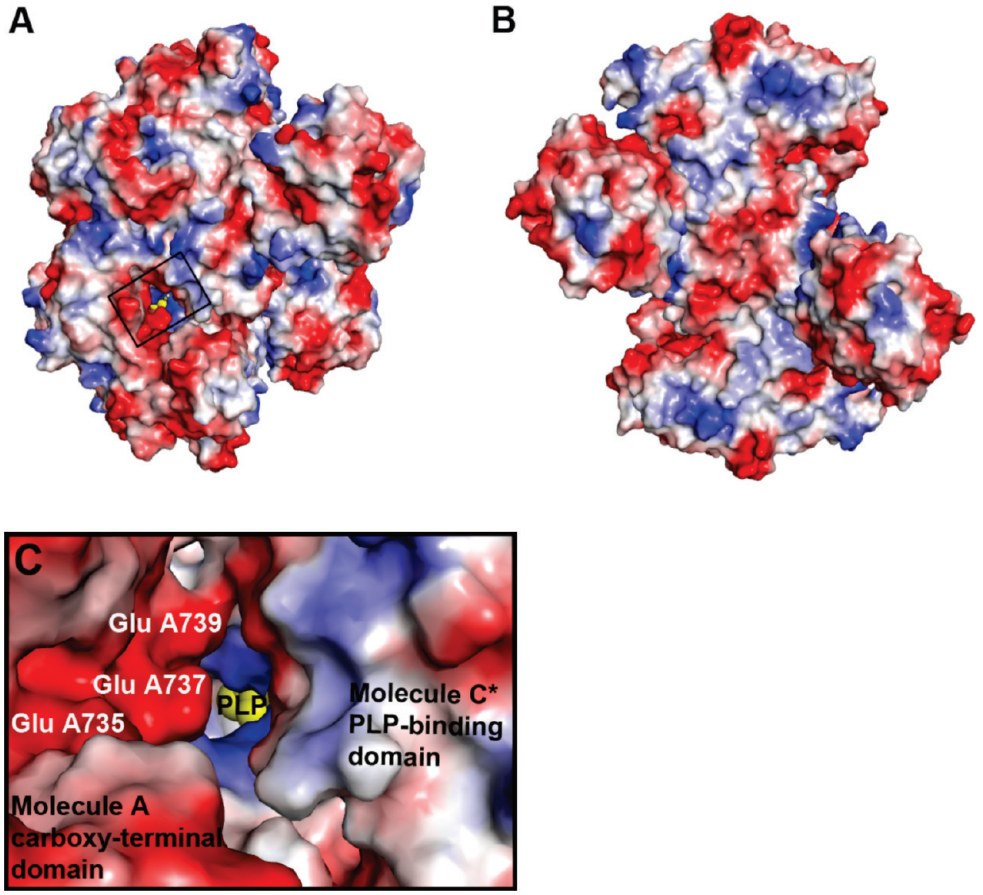


FIGURE 5: Electrostatic surface representation of AdiA AC* homodimer at neutral pH as rendered by Pymol. (A) AdiA homodimer in the same side view orientation as in Figure 2B. The square highlights the active site cleft. (B) 90° rotation around the *y* axis from the orientation in (A). (C) Closer view of the active site cleft between the carboxyl-terminal domain from molecule A and the PLP-binding domain of molecule C*. The cleft is lined with negatively charged residues Glu735, Glu737,and Glu739 along a loop running from the surface to the active site. The PLP cofactor is shown as yellow spheres. Negative electropotential is shown in red, positive electropotential in blue, and neutral in white.

of AdiA at pH 5.2 reflects contributions from two competing factors: conditions under which both Glu739 and Asp202 retain their negative charge for coordination of the substrate and the optimum proportion of acidic surface residues are neutralized to allow assembly of functional AdiA decamers.

*AdiA and OrnDC: Oligomeric States and Substrate Specificities*. AdiA belongs to the family of group III decarboxylases, which includes AdiA, ornithine decarboxylase (OrnDC), and lysine decarboxylase (CadA) (*9*, *10*). The group III decarboxylases use basic amino acid substrates and are large enzymes with approximately 730 amino acids per monomer (*36*, *46*). As the cell pH becomes acidic, AdiA and CadA form decamers as pentamers of dimers and OrnDC forms a dodecamer as a hexamer of dimers (*26*, *36*). Two structures of the *Lactobacillus* 30a OrnDC have been determined: a dodecamer at 3.0 Å resolution (PDB entry 1ORD) (*26*) and a mutant dimer at 2.7 Å resolution (PDB entry 1C4K) (*47*). The higher (2.4 Å) resolution structure of AdiA presented here allows for a more detailed comparison to be made within the group III decarboxylases than has previously been possible.

The monomeric structures of *E. coli* AdiA and the *Lactobacillus* OrnDC are homologous; they have a similar fold and similar domains, and they superpose with an rmsd of 1.74 Å for 649 aligned Cα positions. The main difference between the AdiA and OrnDC structures is their oligomerization state. The wing domains of AdiA and OrnDC mediate different interactions in the AdiA decamer than they do in the OrnDC dodecamer. The OrnDC wing domain lacks the first two α-helices present in the AdiA wing domain. This prevents the OrnDC wing domain from forming the wing−wing contacts seen in AdiA between helices α1 and α2 of neighboring AdiA molecules (Figure 7E,F). The wing−wing interactions in AdiA contribute to tighter packing between monomers, which is necessary for pentameric ring formation (Figure 7C,D). The wing domain of OrnDC, similar to AdiA, packs against the AspAT-like small domain of a neighboring molecule (Figure 7C,D). In contrast to AdiA, the OrnDC wing domain also interacts with the linker domain in the neighboring dimer (Figure 7F). The wing−linker interactions between neighboring dimers in OrnDC are necessary for dodecamer association. A mutation in the linker domain disrupts the packing of adjacent dimers and prevents dodecamer formation, as shown by the Gly121Tyr mutant structure of OrnDC (*47*). OrnDC binds GTP, which activates the OrnDC homodimer (*48*). In contrast, AdiA does not display this type of wing−linker domain packing (Figure 7E), nor does it bind GTP or other nucleotides (*49*). The enzymatic activity of AdiA is dependent on its decamer formation (*12*). In contrast, as a consequence of

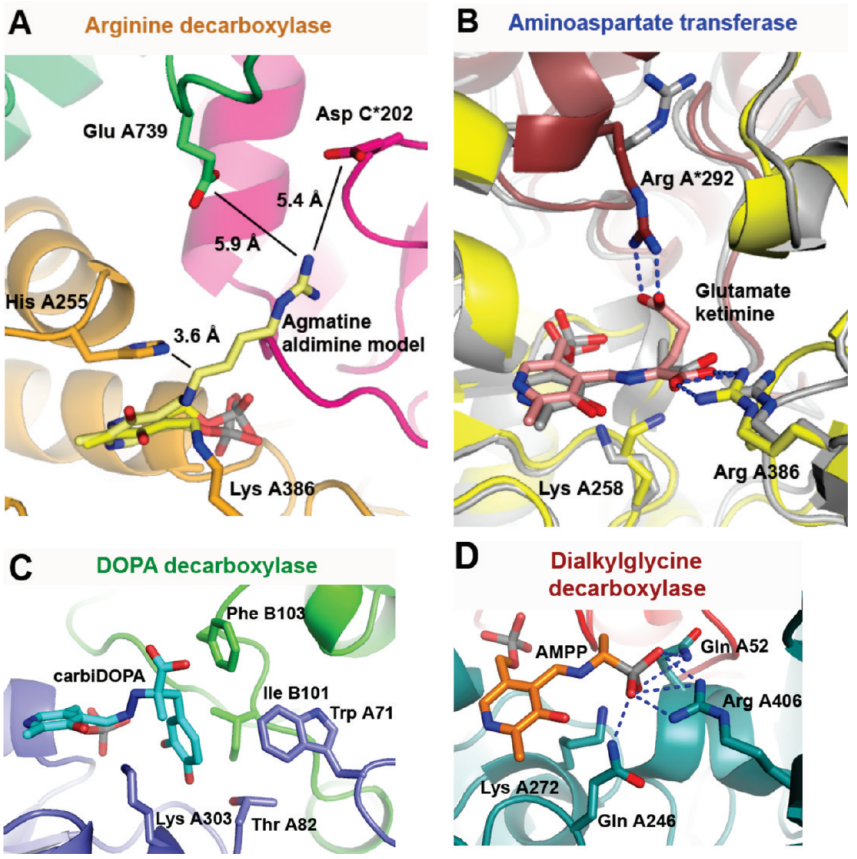


FIGURE 6: AdiA active site modeled with an agmatine aldimine in comparison with substrate- or inhibitor-bound active sites of PLP enzymes. (A) The AdiA active site in the open conformation modeled with an agmatine aldimine. Molecule A PLP-binding domain (orange), molecule C* PLP-binding domain (magenta), molecule A carboxy-terminal domain (green), PLP (yellow), agmatine aldimine model (beige). The distances between side chain groups are indicated by black lines. The pyridine ring of the agmatine aldimine is tilted, which is known to occur in AspAT upon binding of the substrate. The His255 residue is positioned within 4 Å of the Cα atom of the agmatine aldimine. (B) The open and closed conformations of the AspAT active site with bound substrate/substrate analogue (PDB entries 1MAP and 1C9C). Open state dimer with bound substrate analogue (gray), closed state monomer A (yellow), closed state monomer A* (red brown), bound substrate glutamate ketimine (pink). (C) DOPA decarboxylase active site in a closed conformation with bound inhibitor (PDB entry 1JS3). Molecule A (purple), molecule B (green), bound inhibitor carbiDOPA (cyan). Residues from both monomers in the dimer contribute to the binding of the inhibitor. The aromatic ring of the inhibitor is accommodated by a hydrophobic pocket consisting of residues Trp A71, Phe A79 (not shown), Thr A82, Ile B101, and Phe B103. (D) Dialkylglycine decarboxylase active site in a closed conformation with bound aminophosphonate inhibitor (PDB entry 1M0Q). Molecule A (blue green), molecule A* (red), bound AMPP ((*R*)-1-(aminomethyl)propanephosphonate) (orange). The phosphate group of the inhibitor is coordinated by the enzyme in a manner that is likely to resemble that of the coordination of the substrate glycine carboxylate group. In all: nitrogen atoms (blue), oxygen atoms (red), phosphate atoms (gray), and hydrogen bonds are shown as blue dotted lines.

its GTP binding ability, the activity of OrnDC dimers is independent of dodecameric assembly (*47*, *48*). It is not apparent from the structure of the AdiA decamer why the AdiA homodimers are inactive when the decamer is not. It is possible that the AdiA homodimers are inactive because they are structurally unstable. In particular, the protruding wing domains form few interactions with the "core" part of the dimer and are likely to be flexible in solution when not interlocked in the decameric structure by the close packing of the decameric complex. Such structural flexibility of the wing domains could cause long-range conformational changes that affect enzyme activity. The activity of the decamer may thus be a reflection of the increased stability of the homodimers within.

The AdiA and OrnDC active sites superpose well, and the active site residues are conserved (Figure 8). Only one region of the AdiA active site, corresponding to the $\beta$16 strand and the preceding $\alpha$20$-\beta$16 loop in the AspAT-like small domain, shows significant structural differences to the equivalent region in OrnDC. This is due to a shift in the position of the AdiA $\beta$16 strand, which is caused by the preceding $\alpha$20$-\beta$16 loop being two residues shorter than the equivalent loop in OrnDC. Interestingly, the first residue in this $\beta$-strand in OrnDC is Glu532, which has been suggested by Momany et al. to be a determinant of OrnDC substrate specificity by coordinating the $\varepsilon$-amino group of the substrate ornithine aldimine (*26*). The equivalent residue to OrnDC-Glu532 in AdiA is Thr571. The distance between the PLP cofactor and OrnDC-Glu532/AdiA-Thr571 is too short to accommodate an arginine aldimine, which could be why OrnDC shows no activity with arginine as a substrate (*50*). In addition, a threonine residue cannot satisfy the positively charged guanidinium group of the arginine as well as a glutamate or aspartate residue. Hence Thr571 is unlikely to determine substrate specificity in AdiA. The difference in residue identity and the relatively poor structural alignment of the regions around OrnDC-Glu532 and AdiA-Thr571, compared with the bulk of the AdiA and OrnDC active sites, is likely to reflect the different substrate specificities of these decarboxylases.

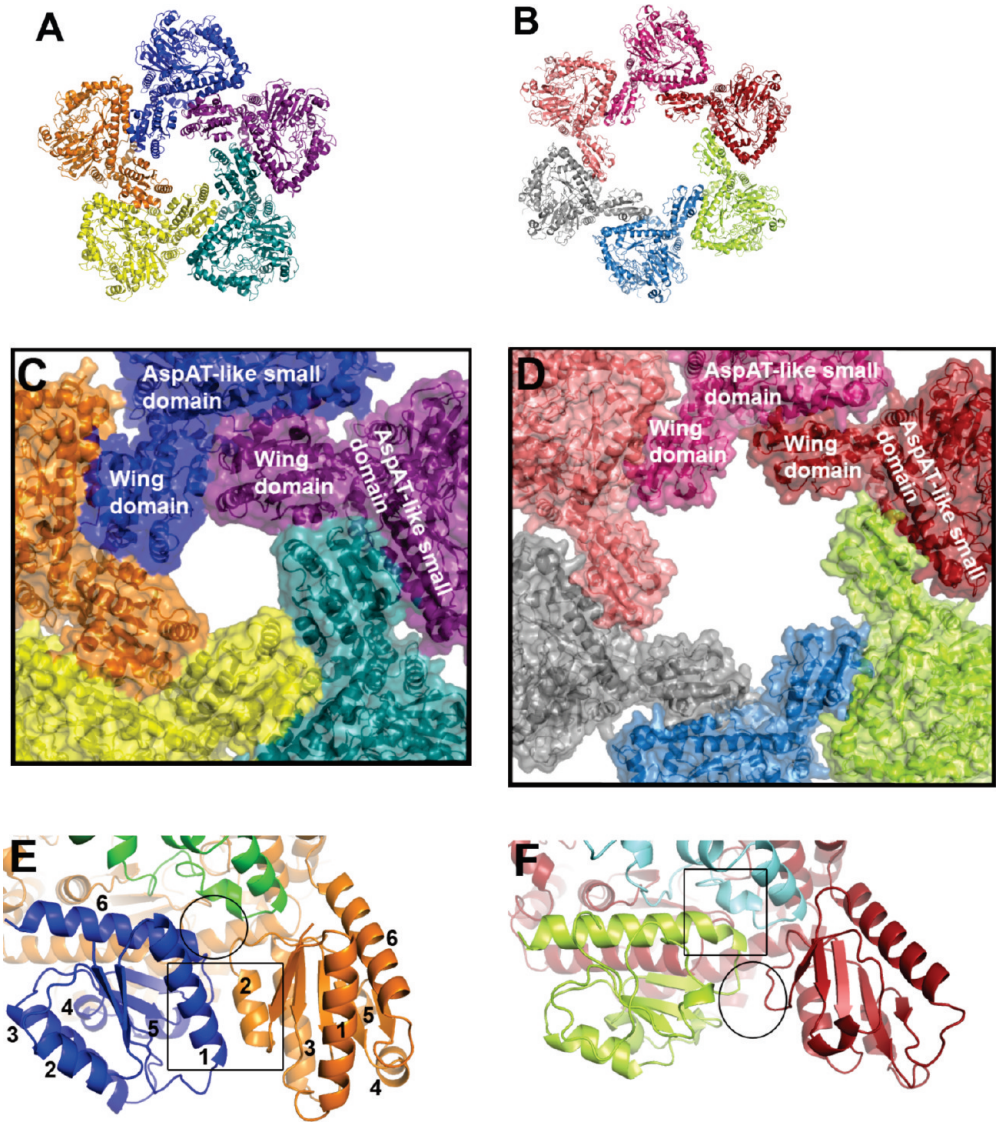


FIGURE 7: Wing domain packing interactions in AdiA and OrnDC. (A) One of the two pentameric rings of the AdiA decamer, bottom view. (B) One of the two hexameric rings of the OrnDC dodecamer, bottom view. (C) The AdiA wing domain packs against the AspAT-like small domain of a neighboring molecule and against two flanking wing domains of neighboring molecules. (D) The OrnDC wing domains pack against the AspAT-like small domain of a neighboring molecule. (E) Two flanking wing domains (molecule A (blue), molecule E (orange)) pack against each other through helix α1 and helix α2, highlighted by a square in the figure. The helices are numbered 1−6 in the N- to C-terminal direction. The molecule A wing domain (blue) makes no interaction with the linker domain from molecule D* (green), part of the ED* dimer, as highlighted in the figure by a circle. (F) The wing domains from neighboring molecules in the OrnDC dodecamer (molecule $A_1$ (lime), molecule $A_2$ (red)) do not form any interactions with each other, as highlighted in the figure by a circle. The molecule $A_1$ wing domain packs against the molecule $B_2$ (cyan) linker domain in the $A_2B_2$ dimer, highlighted by a square in the figure. The view is the same as in (E).

*Comparison of Decarboxylases Important in E. coli Acid Resistance: AdiA and GadB.* The inducible biodegradative glutamate decarboxylase (GadB) is part of the glutamate-dependent acid resistance system (AR2) in *E. coli* (*1*). The principle behind the AR2 system is the same as that of the arginine-dependent acid resistance system (AR3) with a decarboxylase working in tandem with an antiporter. Both AdiA and GadB belong to the type I fold of PLP-dependent enzymes, and as such they both show homology to the PLP-binding domain and the small domain in AspAT. Typically for PLP enzymes both decarboxylases form dimers with the active sites at the dimer interface. Superposing AdiA with GadB (PDB entry 1PMM) (*51*) gave an rmsd of 3.6 Å for 330 aligned Cα atoms. This reflects a gross structural homology between the two enzymes while being consistent with the fact that the sequence identity between GadB and AdiA is only 12%. The main difference between AdiA and GadB, and by extension between group III and group II decarboxylases, is the presence of the wing domain and the carboxy-terminal domain in AdiA. None of the group II decarboxylases for which structures have been determined to date (Table 2) form such large oligomeric assemblies as the AdiA decamer and the OrnDC dodecamer of the group III decarboxylases.

GadB becomes activated and recruited to the membrane at acidic pH (*52*). This has been linked to a conformational change in the structure of the GadB N-terminal chain (*51*, *53*) from a flexible loop at pH 7.6 (PDB entry 1PMO) to a helix at acidic pH 4.6 (PDB entry 1PMM). In the GadB hexamer (PDB entry 1PMM) this helix forms a triple helix bundle that is involved in the

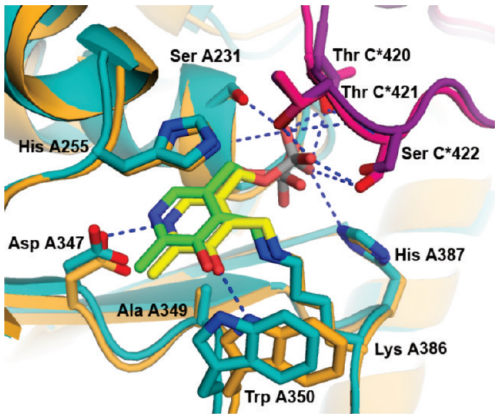


FIGURE 8: Comparison of PLP coordination in the AdiA and OrnDC active sites. The superposition of the AdiA and OrnDC PLP-binding domains (rmsd of 1.8 Å for 242 aligned Cα atoms) illustrates the high degree of conservation of the PLP coordinating residues and the active site between the two decarboxylases. For clarity only the AdiA residues are labeled, and hydrogen bonds are shown in blue dotted lines between the PLP cofactor and the AdiA residues only. AdiA molecule A PLP-binding domain (orange), AdiA molecule C* PLP-binding domain (magenta), PLP cofactor (yellow), OrnDC molecule A PLP-binding domain (cyan), OrnDC molecule B PLP-binding domain (purple), OrnDC-PLP cofactor (green).

recruitment of GadB to the membrane when the cellular pH decreases (*51*). It was suggested that this recruitment to the membrane would allow GadB to more efficiently counter the influx of protons at acidic pH. In contrast, the N-terminus of the AdiA decamer (the active form of the enzyme at acidic pH) forms a wing domain involved in the stabilization of the decameric structure through extensive interactions. The average *B* value of the wing domain (21.8 $Å^2$ in molecule A) compares well with the average *B* value of the molecule as a whole (23.6 $Å^2$ in molecule A). The wing domain is thus unlikely to show conformational flexibility or to undergo a similar structural rearrangement as proposed for the N-terminal domain of GadB. There are no biochemical studies that would confirm whether or not AdiA is recruited to the membrane at acidic pH. However, from comparison of the AdiA and GadB structures, any AdiA recruitment to the membrane at acidic pH would likely occur in a different manner to that of GadB.

## CONCLUSION

The crystal structure of the *E. coli* AdiA presented here is that of a functional decamer, which is an assembly of inactive, homodimeric units. Decamer assembly confers activity by structurally stabilizing the homodimeric units within. It requires neutralization of negatively charged amino acid residues on the wing domains of each monomeric AdiA molecule. Acidic conditions favor this neutralization and therefore decamer assembly. AdiA therefore acts in two ways to consume protons within the cell, through surface charge neutralization and arginine decarboxylation. The pH optimum for AdiA activity reflects a compromise between competing requirements to neutralize surface residues for decamer assembly, while keeping active site residues charged for substrate coordination. By this complex combination of factors, the internal pH of the cell regulates the activity of AdiA.

## REFERENCES

1. Lin, J., Smith, M. P., Chapin, K. C., Baik, H. S., Bennett, G. N., and Foster, J. W. (1996) Mechanisms of acid resistance in enterohemorrhagic *Escherichia coli*. *Appl. Environ. Microbiol. 62* 3094–3100.
2. Gong, S., Richard, H., and Foster, J. W. (2003) YjdE (AdiC) is the arginine:agmatine antiporter essential for arginine-dependent acid resistance in *Escherichia coli*. *J. Bacteriol. 185*, 4402–4409.
3. Iyer, R., Williams, C., and Miller, C. (2003) Arginine-agmatine antiporter in extreme acid resistance in *Escherichia coli*. *J. Bacteriol. 185*, 6556–6561.
4. Auger, E. A., Redding, K. E., Plumb, T., Childs, L. C., Meng, S. Y., and Bennett, G. N. (1989) Construction of lac fusions to the inducible arginine- and lysine decarboxylase genes of *Escherichia coli* K12. *Mol. Microbiol. 3*, 609–620.
5. Eliot, A. C., and Kirsch, J. F. (2004) Pyridoxal phosphate enzymes: mechanistic, structural, and evolutionary considerations. *Annu. Rev. Biochem. 73*, 383–415.
6. Hayashi, H. (1995) Pyridoxal enzymes: mechanistic diversity and uniformity. *J. Biochem. 118*, 463–473.
7. John, R. A. (1995) Pyridoxal phosphate-dependent enzymes. *Biochim. Biophys. Acta 1248*, 81–96.
8. Morris, D. R., and Fillingame, R. H. (1974) Regulation of amino acid decarboxylation. *Annu. Rev. Biochem. 43*, 303–325.
9. Grishin, N. V., Phillips, M. A., and Goldsmith, E. J. (1995) Modeling of the spatial structure of eukaryotic ornithine decarboxylases. *Protein Sci. 4*, 1291–1304.
10. Sandmeier, E., Hale, T. I., and Christen, P. (1994) Multiple evolutionary origin of pyridoxal-5′-phosphate-dependent amino acid decarboxylases. *Eur. J. Biochem. 221*, 997–1002.
11. Richard, H., and Foster, J. W. (2004) *Escherichia coli* glutamate- and arginine-dependent acid resistance systems increase internal pH and reverse transmembrane potential. *J. Bacteriol. 186*, 6032–6041.
12. Boeker, E. A., and Snell, E. E. (1968) Arginine decarboxylase from *Escherichia coli*. II. Dissociation and reassociation of subunits. *J. Biol. Chem. 243*, 1678–1684.
13. Nowak, S., and Boeker, E. A. (1981) The inducible arginine decarboxylase of *Escherichia coli* B: activity of the dimer and the decamer. *Arch. Biochem. Biophys. 207*, 110–116.
14. Studier, F. W., Rosenberg, A. H., Dunn, J. J., and Dubendorff, J. W. (1990) Use of T7 RNA polymerase to direct expression of cloned genes. *Methods Enzymol. 185*, 60–89.
15. Lowry, O. H., Rosebrough, N. J., Farr, A. L., and Randall, R. J. (1951) Protein measurement with the Folin phenol reagent. *J. Biol. Chem. 193*, 265–275.
16. Laemmli, U. K. (1970) Cleavage of structural proteins during the assembly of the head of bacteriophage T4. *Nature (London) 227*, 680–685.
17. Jancarick, J., and Kim, S. H. (1991) Sparse matrix sampling: a screening method for crystallisation of proteins. *J. Appl. Crystallogr. 24*, 409–411.
18. Otwinowski, Z., and Minor, W. (1997) Processing of X-ray diffraction data collected in oscillation mode. *Methods Enzymol., Part A 276*, 307–326.
19. Uson, I., and Sheldrick, G. M. (1999) Advances in direct methods for protein crystallography. *Curr. Opin. Struct. Biol. 9*, 643–648.
20. Bricogne, G., Vonrhein, C., Flensburg, C., Schiltz, M., and Paciorek, W. (2003) Generation, representation and flow of phase information in structure determination: recent developments in and around SHARP 2.0. *Acta Crystallogr., Sect. D: Biol. Crystallogr. 59*, 2023–2030.
21. Terwilliger, T. C. (2000) Maximum-likelihood density modification. *Acta Crystallogr., Sect. D: Biol. Crystallogr. 56*, 965–972.
22. Cowtan, K. (1994) An automated procedure for phase improvement by density modification. *Joint CCP4 ESF-EACBM Newsl. Protein Crystallogr. 31*, 34–38.
23. Cowtan, K. (2006) The Buccaneer software for automated model building. 1. Tracing protein chains. *Acta Crystallogr., Sect. D: Biol. Crystallogr. 62*, 1002–1011.
24. Perrakis, A., Morris, R., and Lamzin, V. S. (1999) Automated protein model building combined with iterative structure refinement. *Nat. Struct. Biol. 6*, 458–463.
25. Emsley, P., and Cowtan, K. (2004) Coot: model-building tools for molecular graphics. *Acta Crystallogr., Sect. D: Biol. Crystallogr. 60*, 2126–2132.
26. Momany, C., Ernst, S., Ghosh, R., Chang, N. L., and Hackert, M. L. (1995) Crystallographic structure of a PLP-dependent ornithine decarboxylase from *Lactobacillus* 30a to 3.0 Å resolution. *J. Mol. Biol. 252*, 643–655.

27. Schwarzenbacher, R., Godzik, A., Grzechnik, S. K., and Jaroszewski, L. (2004) The importance of alignment accuracy for molecular replacement. *Acta Crystallogr., Sect. D: Biol. Crystallogr. 60*, 1229–1236.
28. Murshudov, G. N., Vagin, A. A., and Dodson, E. J. (1997) Refinement of macromolecular structures by the maximum-likelihood method. *Acta Crystallogr., Sect. D: Biol. Crystallogr. 53*, 240–255.
29. Painter, J., and Merritt, E. A. (2006) Optimal description of a protein structure in terms of multiple groups undergoing TLS motion. *Acta Crystallogr., Sect. D: Biol. Crystallogr. 62*, 439–450.
30. Shah, R., Akella, R., Goldsmith, E. J., and Phillips, M. A. (2007) X-ray structure of *Paramecium bursaria* Chlorella virus arginine decarboxylase: insight into the structural basis for substrate specificity. *Biochemistry 46*, 2831–2841.
31. Davis, I. W., Leaver-Fay, A., Chen, V. B., Block, J. N., Kapral, G. J., Wang, X., Murray, L. W., Arendall, W. B.III, Snoeyink, J., Richardson, J. S., and Richardson, D. C. (2007) MolProbity: all-atom contacts and structure validation for proteins and nucleic acids. *Nucleic Acids Res. 35*, W375–W383.
32. Krissinel, E., and Henrick, K. (2004) Secondary-structure matching (SSM), a new tool for fast protein structure alignment in three dimensions. *Acta Crystallogr., Sect. D: Biol. Crystallogr. 60*, 2256–2268.
33. Boeker, E. A., Fischer, E. H., and Snell, E. E. (1969) Arginine decarboxylase from *Escherichia coli*. 3. Subunit structure. *J. Biol. Chem. 244*, 5239–5245.
34. Boeker, E. A. (1978) Arginine decarboxylase from *Escherichia coli* B: mechanism of dissociation from the decamer to the dimer. *Biochemistry 17*, 258–263.
35. Frieden, C. (1971) Protein-protein interaction and enzymatic activity. *Annu. Rev. Biochem. 40*, 653–696.
36. Sabo, D. L., and Fischer, E. H. (1974) Chemical properties of *Escherichia coli* lysine decarboxylase including a segment of its pyridoxal 5′-phosphate binding site. *Biochemistry 13*, 670–676.
37. Bonisch, H., Schmidt, C. L., Schafer, G., and Ladenstein, R.(2002) The structure of the soluble domain of an archaeal Rieske iron-sulfur protein at 1.1 Å resolution. *J. Mol. Biol. 319*, 791–805.
38. Cooper, J. B., Khan, G., Taylor, G., Tickle, I. J., and Blundell, T. L. (1990) X-ray analyses of aspartic proteinases. II. Three-dimensional structure of the hexagonal crystal form of porcine pepsin at 2.3 Å resolution. *J. Mol. Biol. 214*, 199–222.
39. Fushinobu, S., Ito, K., Konno, M., Wakagi, T., and Matsuzawa, H. (1998) Crystallographic and mutational analyses of an extremely acidophilic and acid-stable xylanase: biased distribution of acidic residues and importance of Asp37 for catalysis at low pH. *Protein Eng. 11*, 1121–1128.
40. Kashiwagi, T., Kunishima, N., Suzuki, C., Tsuchiya, F.Nikkuni, S., Arata, Y., and Morikawa, K. (1997) The novel acidophilic structure of the killer toxin from halotolerant yeast demonstrates remarkable folding similarity with a fungal killer toxin. *Structure 5*, 81–94.
41. Akhtar, M., Stevenson, D. E., and Gani, D. (1990) Fern L-methionine decarboxylase: kinetics and mechanism of decarboxylation and abortive transamination. *Biochemistry 29*, 7648–7660.
42. Gani, D. (1991) A structural and mechanistic comparison of pyridoxal 5′-phosphate dependent decarboxylase and transaminase enzymes. *Philos. Trans. R. Soc. London, Ser. B 332*, 131–139.
43. Ishii, S., Mizuguchi, H., Nishino, J., Hayashi, H., and Kagamiyama, H. (1996) Functionally important residues of aromatic L-amino acid decarboxylase probed by sequence alignment and site-directed mutagenesis. *J. Biochem. 120*, 369–376.
44. Bertoldi, M., Castellani, S., and Bori Voltattorni, C. (2001) Mutation of residues in the coenzyme binding pocket of Dopa decarboxylase. Effects on catalytic properties. *Eur. J. Biochem. 268* 2975–2981.
45. Malashkevich, V. N., Toney, M. D., and Jansonius, J. N. (1993) Crystal structures of true enzymatic reaction intermediates: aspartate and glutamate ketimines in aspartate aminotransferase. *Biochemistry 32*, 13451–13462.
46. Morris, D. R., and Boeker, E. A. (1983) Biosynthetic and biodegradative ornithine and arginine decarboxylases from *Escherichia coli*. *Methods Enzymol. 94*, 125–134.
47. Vitali, J., Carroll, D., Chaudhry, R. G., and Hackert, M. L. (1999) Three-dimensional structure of the Gly121Tyr dimeric form of ornithine decarboxylase from *Lactobacillus* 30a. *Acta Crystallogr., Sect. D: Biol. Crystallogr. 55*, 1978–1985.
48. Oliveira, M. A., Carroll, D., Davidson, L., Momany, C., and Hackert, M. L. (1997) The GTP effector site of ornithine decarboxylase from *Lactobacillus* 30a: kinetic and structural characterization. *Biochemistry 36*, 16147–16154.
49. Applebaum, D. M., Dunlap, J. C., and Morris, D. R. (1977) Comparison of the biosynthetic and biodegradative ornithine decarboxylases of *Escherichia coli*. *Biochemistry 16*, 1580–1584.
50. Guirard, B. M., and Snell, E. E. (1980) Purification and properties of ornithine decarboxylase from *Lactobacillus* sp. 30a. *J. Biol. Chem. 255*, 5960–5964.
51. Capitani, G., De Biase, D., Aurizi, C., Gut, H., Bossa, F., and Grutter, M. G. (2003) Crystal structure and functional analysis of *Escherichia coli* glutamate decarboxylase. *EMBO J. 22* 4027–4037.
52. Capitani, G., Tramonti, A., Bossa, F., Grutter, M. G., and De Biase, D. (2003) The critical structural role of a highly conserved histidine residue in group II amino acid decarboxylases. *FEBS Lett. 554* 41–44.
53. Gut, H., Pennacchietti, E., John, R. A., Bossa, F., Capitani, G., De Biase, D., and Grutter, M. G. (2006) *Escherichia coli* acid resistance: pH-sensing, activation by chloride and autoinhibition in GadB. *EMBO J. 25*, 2643–2651.
54. Malashkevich, V. N., Kochkina, V. M., Torchinskii Iu, M., and Arutiunian, E. G. (1982) Conformational changes in cytosol aspartate aminotransferase induced by oxoglutarate. *Dokl. Akad. Nauk SSSR 267*, 1257–1261.
55. Toney, M. D., Hohenester, E., Cowan, S. W., and Jansonius, J. N. (1993) Dialkylglycine decarboxylase structure: bifunctional active site and alkali metal sites. *Science 261*, 756–759.
56. Burkhard, P., Dominici, P., Borri-Voltattorni, C., Jansonius, J. N., and Malashkevich, V. N. (2001) Structural insight into Parkinson's disease treatment from drug-inhibited DOPA decarboxylase. *Nat. Struct. Biol. 8*, 963–967.
57. Fenalti, G., Law, R. H., Buckle, A. M., Langendorf, C., Tuck, K., Rosado, C. J., Faux, N. G., Mahmood, K., Hampe, C. S., Banga, J. P., Wilce, M., Schmidberger, J., Rossjohn, J., El-Kabbani, O., Pike, R. N., Smith, A. I., Mackay, I. R., Rowley, M. J., and Whisstock, J. C. (2007) GABA production by glutamic acid decarboxylase is regulated by a dynamic catalytic loop. *Nat. Struct. Mol. Biol. 14*, 280–286.
58. Toney, M. D. (2005) Reaction specificity in pyridoxal phosphate enzymes. *Arch. Biochem. Biophys. 433*, 279–287.